Determining the translational and internal temperatures of isolated metal clusters: A comprehensive approach based on molecular-beam-deflection experiments

Thomas M. Fuchs,* Filip Rivic, and Rolf Schäfer

Eduard-Zintl-Institut für Physikalische und Anorganische Chemie, Technische Universität Darmstadt, Alarich-Weiss-Straße 8, 64287 Darmstadt, Germany

(Received 11 May 2021; revised 25 June 2021; accepted 14 July 2021; published 30 July 2021)

An approach to translational, rotational, and vibrational temperatures of small metal clusters (Ga_MSn_N, $M = 0, 1$ and $N = 6$–16) in a molecular beam from a cryogenically cooled laser vaporization source is presented. The velocity distribution in the molecular beam is measured with a mechanical shutter at a fixed photoionization delay which gives an estimate of the lower bound of the translational temperature T_{trans}. These values of T_{trans} are found to be considerably smaller than the corresponding nozzle temperatures $T_{nozzle} = 16$–300 K. The rotational temperature T_{rot} is estimated from the comparison of an electric deflection experiment with molecular dynamics simulations and from magnetic deflection experiments to be in the range $T_{rot} = 5$–20 K for $T_{nozzle} = 16$ K. The vibrational temperature T_{vib} is studied by comparing magnetic deflection experiments with a microscopic model based on avoided level crossings between vibrational, rotational, and Zeeman energy levels. For $T_{nozzle} \geqslant 50$ K, $T_{vib} \approx T_{nozzle}$ is observed, while for lower temperatures, $T_{vib} > T_{nozzle}$. Thus, $T_{trans} \leqslant T_{rot} < T_{vib}$ is found at least for $N = 11, 12$ and the lowest nozzle temperature of 16 K.

DOI: 10.1103/PhysRevA.104.012820

I. INTRODUCTION

Forty years after the invention of the laser vaporization source for the production of molecular beams of metal clusters, the determination of cluster temperatures is still a formidable task [1–3]. Since the generated clusters are isolated in the molecular beam and therefore have no contact with a heat bath, the temperature of the clusters is initially not fixed. In particular, it cannot be assumed that the different degrees of freedom of the clusters are in thermal equilibrium with one another. Nevertheless, there is a great deal of evidence that clusters in the molecular beam can be thermally excited and that this thermal excitation is then also reflected in the experimental observations. The thermal excitation, for example, has great impact on electric and magnetic deflection experiments [4–6], absorption spectra [7,8], or the calorimetric investigation of isolated clusters [9]. Therefore, it is indeed meaningful to describe the thermal excitation in the isolated clusters by a temperature. However, each degree of freedom must be characterized by its own temperature.

In a typical pulsed cluster source, metal clusters are formed by condensation when a plasma of metal vapor is cooled down in a carrier gas (mostly helium). The helium-cluster mixture then flows through a nozzle which can be cooled down to cryogenic temperatures and expands into high vacuum. Inside the nozzle, the pressure of the inert gas p is large enough (typically in the range of a few millibars [10]) to control the thermal excitation of the clusters by collisions with the carrier gas, which is itself thermalized with the nozzle by wall collisions. The cross section σ for energy transfer from vibrational, rotational, and translational degrees of freedom follows the order $\sigma_{vib} \ll \sigma_{rot} < \sigma_{trans}$ [11,12]. Therefore, it is usually observed that translations and rotations are readily thermalized inside the nozzle. This need not be the case for the vibrational modes of the cluster. From molecular dynamics simulations it can be estimated that for an equilibration of the vibrational degrees of freedom with the nozzle, a few thousand collisions are necessary [13]. A simple gas kinetic approach can be used to estimate the number of collisions with the carrier gas in the nozzle. For a He pressure of $p = 5$ mbar, a collision frequency of 2×10^9 s^{-1} results if a typical value for the collision cross section of 1 nm^2 [14], as well as the reduced mass $\mu \approx m_{He}$, and a nozzle temperature T_{nozzle} of 20 K is considered [15,16]. The dwell time, i.e., the time span from laser vaporization to nozzle exit, is in the range of 1 ms, which means that the total number of collisions is about 2×10^6. Most of the collisions occur in the gas aggregation chamber and only a fraction in the cryogenically cooled nozzle extension because the diameter of the latter is smaller and thus the helium-cluster mixture already gets accelerated. Taking the inner dimensions of the gas aggregation chamber and the nozzle in our apparatus into account, about 10^4 of the helium-cluster collisions occur in the cold nozzle. Still, this number should be large enough to ensure complete cluster thermalization, i.e., also the vibrational degrees of freedom should be thermalized by collisions with the inert carrier gas. After passing the nozzle, the helium-cluster mixture expands adiabatically into high vacuum, which leads to further cooling. Again, because of the more effective energy transfer from translational and rotational degrees of freedom to He atoms compared to the energy transfer from vibrations, the translational and rotational degrees of freedom are cooled more effectively than the vibrational ones, i.e., $T_{trans}, T_{rot} < T_{vib}$

*thomas.fuchs@tu-darmstadt.de

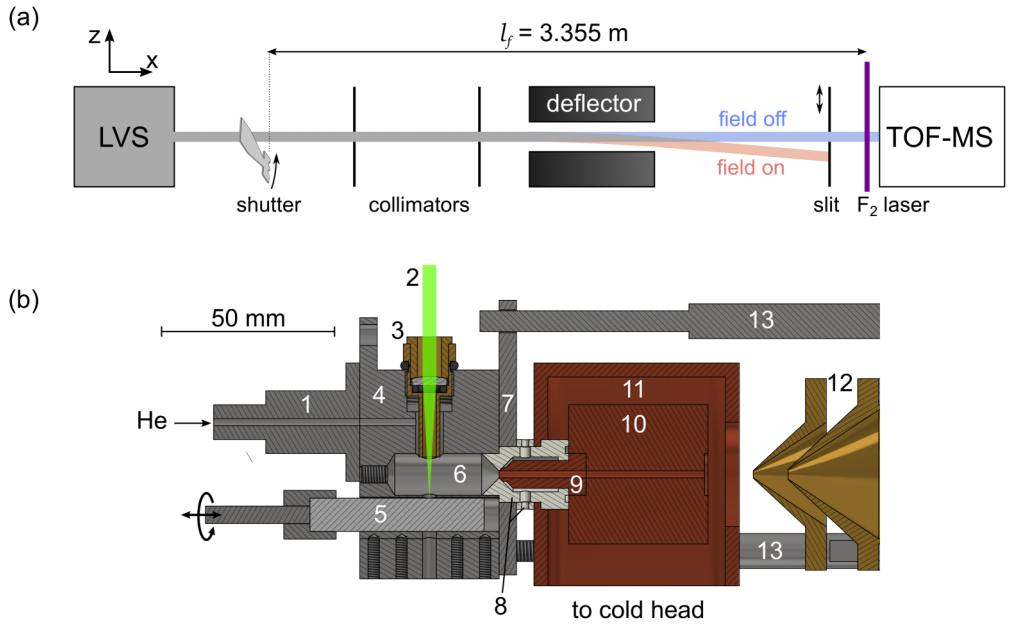

FIG. 1. (a) Scheme of the molecular-beam-deflection apparatus containing a laser vaporization source (LVS), a mechanical shutter, two collimators, a deflector (inhomogeneous electric or magnetic field), the ionization laser beam (purple), a scanning slit, and a time-of-flight mass spectrometer (TOF-MS). (b) Technical drawing (to scale) of the LVS equipped with a cryogenically cooled nozzle used to generate pulsed molecular beams of cold metal clusters: 1, pulsed solenoid valve; 2, second harmonic of a pulsed Nd:YAG laser; 3, focusing lens in a brass bracket; 4, source body (stainless steel); 5, target rod mounted on a rotating and translating drive shaft; 6, aggregation chamber; 7, mounting plate for cryogenic nozzle (stainless steel); 8, thermal isolation (Torlon); 9, cryogenic nozzle extension oxygen-free high-thermal-conductivity (OFHC) copper; 10, cryogenic nozzle (OFHC copper); 11, radiation shield (OFHC copper); 12, double-skimmer arrangement (brass); and 13, stud bolts holding the mounting plate (7).

after the adiabatic expansion. The extent of cooling depends sensitively on the expansion conditions, especially the helium backing pressure and nozzle dimensions [17,18]. Therefore, the temperatures of the various degrees of freedom are *a priori* unknown. However, knowledge of the clusters temperatures is essential, particularly for the analysis of molecular-beam-deflection experiments.

The temperature in supersonic molecular beams was studied with spectroscopic methods for some molecules but only very small cluster species like dimers and trimers. It was found that the vibrational degrees of freedom are thermalized with the beam nozzle but not cooled further in the expansion while translational and also rotational degrees of freedom are usually cooled significantly, depending sensitively on the backing pressure of the carrier gas and the nozzle dimensions. Thus, $T_{\rm trans} \leqslant T_{\rm rot} \ll T_{\rm vib}$ was observed. For example, Hopkins *et al.* found $T_{\rm trans} < 6\,{\rm K}$, $T_{\rm rot} = 5\,{\rm K}$, and $T_{\rm vib} \approx 325\,{\rm K}$ with resonant two-photon ionization for Mo_2 from a laser vaporization at room temperature [19]. However, the high-resolution spectroscopic method used for the Mo dimer cannot be applied easily to larger clusters containing heavy metal atoms because the resolution of spectroscopic features is far more difficult. The largest metal clusters for which vibrational resolution was achieved in electronic spectra are Ni_3 [20], coinage metal trimers [21–23], Bi_3 [24], Cu_4^+ [25], and Au_4^+ [26]. Here it was also estimated that $T_{\rm vib}$ is close to the nozzle temperature, eventually a bit higher. The same was found in delayed ionization studies on small Nb clusters [27] and Stern-Gerlach experiments on $MnSn_{12}$ [5]. Rotationally resolved spectra were only observed for very small species like coinage metal dimers [28–30] or the light alkali-metal clusters Li_3 [31,32] and Na_3 [33]. Therein, rotational temperatures of about 10–20 K were reported for dimers and trimers from hot oven sources.

The deflection in electric and magnetic fields can be utilized to study the vibrational and rotational temperatures for larger clusters. Since the approach for the determination of $T_{\rm vib}$ and $T_{\rm rot}$ from deflection experiments has not yet been described in detail, we want to present the procedure explicitly in this paper. For this purpose, a lower limit to $T_{\rm trans}$ and the values for $T_{\rm rot}$ and $T_{\rm vib}$ are systematically determined for $GaSn_N$ and Sn_N ($N = 6$–16) clusters from electric and magnetic deflection experiments and a measurement of the velocity distribution in the beam. The nozzle temperature is varied over a large range from 16 K up to room temperature. These experiments are all carried out in the same apparatus, thus ensuring that the cluster source conditions are comparable and the results are discussed with respect to previous findings. In earlier experiments with our cluster source, it was found that the values of $T_{\rm rot}$ are smaller than the nozzle temperature $T_{\rm nozzle}$, but $T_{\rm vib} \approx T_{\rm nozzle}$ for $T_{\rm nozzle}$ larger than 30–50 K [34–37].

II. EXPERIMENTAL DETAILS

A. Molecular-beam apparatus

The apparatus used here is shown schematically in Fig. 1(a). It differs only in details from our earlier works [36,38,39]. Nevertheless, as the design of the laser vaporization source [see Fig. 1(b)] is crucial for cluster formation

and thermalization, it will be discussed in some detail here. A frequency-doubled Nd:YAG laser (2) (532 nm, 10 Hz, about 20–30 mJ per pulse) is focused onto a rotating and translating alloyed target rod (5) containing 5 at. % Ga in Sn (Alfa Aesar, 99.98% purity), ablating a small amount of material. The emerging plasma is cooled down in a short helium pulse (about 400 μs) from a solenoid valve (1) (Parker Series 9, He backing pressure of 6.5 bars) which facilitates cluster aggregation. The helium-cluster mixture streams from the aggregation chamber (6) (12 mm diameter, temperature 275–300 K) into the cryogenically cooled nozzle (9 and 10), which has an inner diameter of 2 mm and a length of 59 mm. The nozzle is insulated against the mounting plate (7) by a small Torlon (polyamide-imide) piece (8) and enclosed by a radiation shield (11). The first stage of the cold head of a closed cycle helium cryocooler (Sumitomo RDK-408D2) is coupled to the radiation shield and the second stage to the cryogenic nozzle via oxygen-free high-thermal-conductivity copper braids. The nozzle temperature is measured with a silicon diode (DT-670B-CU) located on the nozzle body on the opposite side from the cold head connection. The temperature is controlled by a Lakeshore TC325 with a heater cartridge (50 W). The nozzle can be cooled down to 8 K; however, molecular-beam stability becomes significantly worse below 15 K. The cold helium-cluster mixture expands into high vacuum and passes a double-skimmer arrangement (12). About 160 mm downstream the nozzle opening, the molecular beam can be chopped using a mechanical shutter based on a hard disk drive to determine cluster velocities [40,41]. Then the molecular beam is collimated to a rectangular shape of 0.2×2 mm^2 and deflected in an inhomogeneous electric or magnetic field to probe the Stark or Zeeman effect, respectively. To record beam deflection profiles, a 400-μm broad slit is scanned over the molecular-beam profile in deflection direction. The neutral clusters are ionized with an F_2 excimer laser (157 nm, Coherent Excistar XS200) and analyzed in a time-of-flight mass spectrometer which is aligned orthogonal to both the beam propagation (x axis) and beam deflection direction (z axis).

The measured deflection d in both electric ($|\mathbf{E}| = E \equiv \Gamma_{\mathrm{el}}$) and magnetic fields ($|\mathbf{B}| = B \equiv \Gamma_{\mathrm{mag}}$) depends on cluster mass m_{cluster}, velocity v_x, apparatus constant A, and field gradient according to

$$d = \frac{A}{m v_x^2} \frac{d\Gamma_i}{dz} \overline{\mu}_{z,i}, \tag{1}$$

with $i \in \{\mathrm{el,mag}\}$. In the beam profiles shown in Secs. V and VI, the measured deflections are converted to the average projection of the dipole moment on the field axis during the gradient field passage $\overline{\mu}_{z,i}$ to eliminate the dependence on cluster mass, velocity, and apparatus specific constants. However, it should be mentioned that the shown beam profiles are not directly the dipole moment distribution but its convolution with the initial molecular-beam width which determines the spatial resolution of the experiment.

B. Determination of the cluster velocity

The velocity distribution $F(v_x)$ of the clusters in the molecular beam is determined from the flight time t_f and the distance between the mechanical shutter and the ionization position l_f [see Fig. 1(a)]. The shutter closing time t_{shutter} is tracked during the experiment with a light barrier. The shot time of the excimer laser t_{exc} is determined from the laser trigger time and the delay from trigger to laser shot, which is about 70 μs. The beam intensity is measured for a series of shutter closing times which are converted to the corresponding velocities $v_x = l_f/t_f = l_f/(t_{\mathrm{exc}} - t_{\mathrm{shutter}})$ to get the integrated cluster velocity distribution in Fig. 2. Note that, strictly speaking, the convolution of the cluster velocity distribution with the shutter closing function is measured because of the nonzero width of the molecular beam and the finite shutter arm velocity. However, the contribution of the latter is small. Typical mean values for t_f are 3–8 ms (depending on T_{nozzle}) and most clusters are found in a range of 0.2–0.4 ms. The shutter arm chops the molecular beam with a velocity of 3.5 ms^{-1} along the 0.2-mm narrow side of the molecular beam, which means that the chopper covers the beam in less than 0.1 ms. The jitter of the hard disk drive shutter is smaller than 1 μs and the drift of the shutter closing time during the experiment is smaller than 10 μs. The jitter of t_{exc} is in the nanosecond range and can be neglected. The major part of the uncertainty of the determined values of v_x is due to the calibration procedure of the shutter closing time. This is done by coupling a continuous laser beam onto the molecular-beam axis and measuring the chopped light signal in comparison to the permanently installed light barrier. The expected uncertainty of laser alignment causes an uncertainty of v_x of about 3% [39].

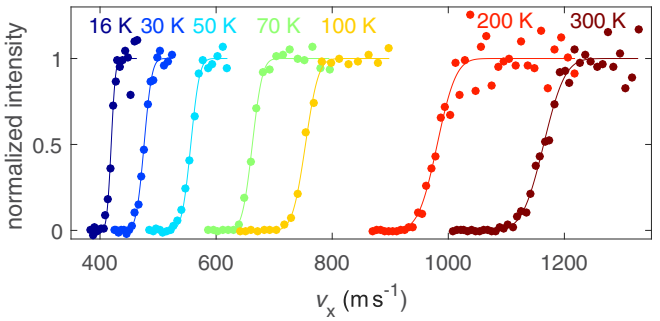

FIG. 2. Measured integrated velocity distribution for Sn_{12} clusters for nozzle temperatures from 16 to 300 K with error function fit [Eq. (2)].

The velocity distribution in seeded molecular beams can generally be described by a modified Gaussian function. For Mach numbers $M \gg 1$, the shape of the velocity distribution is described well by a simple Gaussian function [42,43]. For the clusters in our molecular beam, the Mach numbers are at least 50. Thus, the ensemble average $\langle v_x \rangle$ and the value of T_{trans} are determined from fitting an error function

$$F(v_x) \propto 1 + \mathrm{erf}\left(\frac{v_x - \langle v_x \rangle}{\alpha}\right), \tag{2}$$

with $\alpha = \sqrt{2 k_B T_{\mathrm{trans}}/m_{\mathrm{cluster}}}$ to the experimentally determined integrated velocity distributions. Note that only the velocity and translational temperature in beam propagation direction are measured here.

C. Influence of fixed photoionization delay

It is important to note that the values of T_{trans} determined by the method described in the preceding section are not the translational temperature of the whole molecular beam but a temperature describing the width of the velocity distribution of the detected clusters only. In most molecular-beam experiments designed for studying the properties of small metal clusters, not all of the clusters leaving the source are studied. When clusters with different velocities v_x leave the source at some point in time, the beam will spread along the beam propagation direction and only a narrow section of the beam is detected in the commonly used orthogonal time-of-flight mass spectrometers. The width of this section is limited by the size of the acceleration field, the active area of the ion detector, or in our case the width of the photoionization laser beam, which measures 3–5 mm. In other words, only clusters that are at the location where the molecular beam crosses the ionization laser at the point of time when the laser fires contribute to the measured velocity distributions and deflection profiles. All other clusters, which are too slow or fast or left the cluster source too early or late are omitted. Therefore, the velocity distribution we measure is more narrow and the determined values of T_{trans} should be understood as a lower bound to the actual temperature. However, because in most experiments also only a small portion of the molecular beam is investigated, this approach seems useful when information on cluster velocity distribution is needed for the interpretation of experimental results. It is relevant, for example, for estimating the influence of the velocity spread on the cluster deflection through Eq. (1). The total width of the velocity distribution for all clusters in the beam does not play a role here because the fastest and slowest clusters are not detected. While the velocity distribution of the whole beam is useful for a detailed cluster source characterization and the study of translational cooling in the adiabatic expansion [43], our approach is advantageous for the analysis of molecular-beam experiments like determining electric and magnetic moments from deflection experiments.

III. COMPUTATIONAL DETAILS

In order to extract the vibrational and rotational temperatures from the analysis of the experimental data, the values of the electric dipole moment μ_{el}, rotational constant B_{rot}, and vibrational modes ν_i are calculated with quantum chemical methods. Global structure optimizations were carried out with a pool-genetic algorithm (GA) based on the Birmingham cluster genetic algorithm to predict the structures of the $GaSn_N$ clusters [44]. For this, an initial pool of ten random structures is generated by the program. The GA is coupled with the plane-wave self-consistent-field density-functional-theory module of the QUANTUMESPRESSO package [45]. A total number of 36 core electrons of tin and 18 core electrons of the gallium atom are described by the Uutrasoft Rabe-Rappe-Kaxiras-Joannopoulos pseudopotentials [46], while the rest of the electrons are calculated explicitly with the Perdew-Burke-Ernzerhof (PBE) exchange-correlation functional [47]. For this, an energy cutoff of 30 Ry is chosen and an additional Methfessel-Paxton smearing [48] is applied to improve convergence. Total energy and force convergence thresholds of 10^{-4} eV and 10^{-3} eV Å^{-1}, respectively, are chosen for the optimization steps within the GA calculation. We assume that a pool is converged when no new global minimum (GM) is found within 1000 new generated structures. The final pool structures are then sorted depending on their energies and moments of inertia and locally optimized with the PBE0 functional [49] and def2-TZVPP basis set [50]. This level of theory has proven to give reliable results for small tin clusters with different dopant atoms [51,52]. Additionally, an effective small-core pseudopotential is applied for the core electrons of tin. The local optimization and calculation of the electric dipole moment are carried out with the quantum chemical program NWCHEM [53]. Analytic vibrational modes of the locally optimized structures are calculated with ORCA [54].

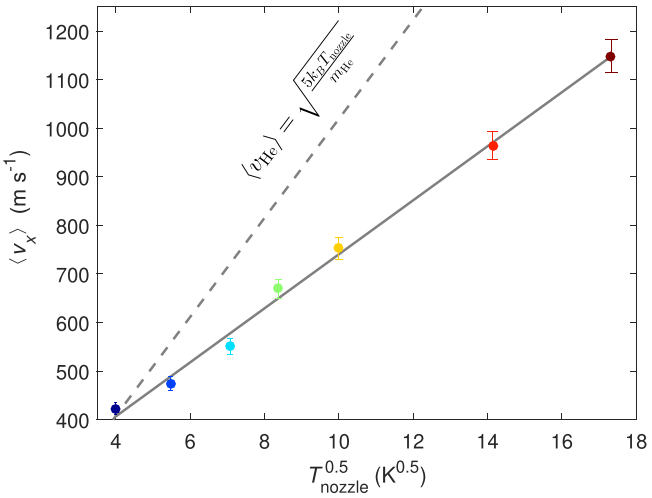

FIG. 3. Average velocity $\langle v_x \rangle$ against the square root of the nozzle temperature. The course of the velocities is similar for all investigated clusters. The solid line shows a linear fit and the dashed line the maximum velocity for a monatomic gas $\langle v_{\text{He}} \rangle = \sqrt{5k_B T_{\text{nozzle}}/m_{\text{He}}}$ [15].

IV. TRANSLATIONS

A. Average cluster velocity $\langle v_x \rangle$

Figure 2 shows the measured integrated velocity distributions and error function fits for Sn_{12} for values of T_{nozzle} from 16 to 300 K. The resulting average cluster velocities $\langle v_x \rangle$ in Fig. 3 scale with the square root of the nozzle temperature $\sqrt{T_{\text{nozzle}}}$. For the lowest nozzle temperature of 16 K, the cluster velocity coincides with the maximum terminal velocity of a monatomic gas, which is given by $\langle v_{\text{He}} \rangle = \sqrt{5k_B T_{\text{nozzle}}/m_{\text{He}}}$ [15] (dashed gray line in Fig. 3). However, the cluster velocity becomes increasingly smaller than this for larger values of T_{nozzle}, i.e., there is a significant velocity slip.

The measured average velocities $\langle v_x \rangle$ for all cluster species present in the molecular beam are shown in Fig. 4. The value of $\langle v_x \rangle$ decreases for increasing cluster mass, which is in line with observations on similar laser vaporization sources [43,55]. This trend is more pronounced for the higher values of T_{nozzle}. The solid and dashed lines in Fig. 4 are fits of a flow model developed by van der Tol and Janssens which

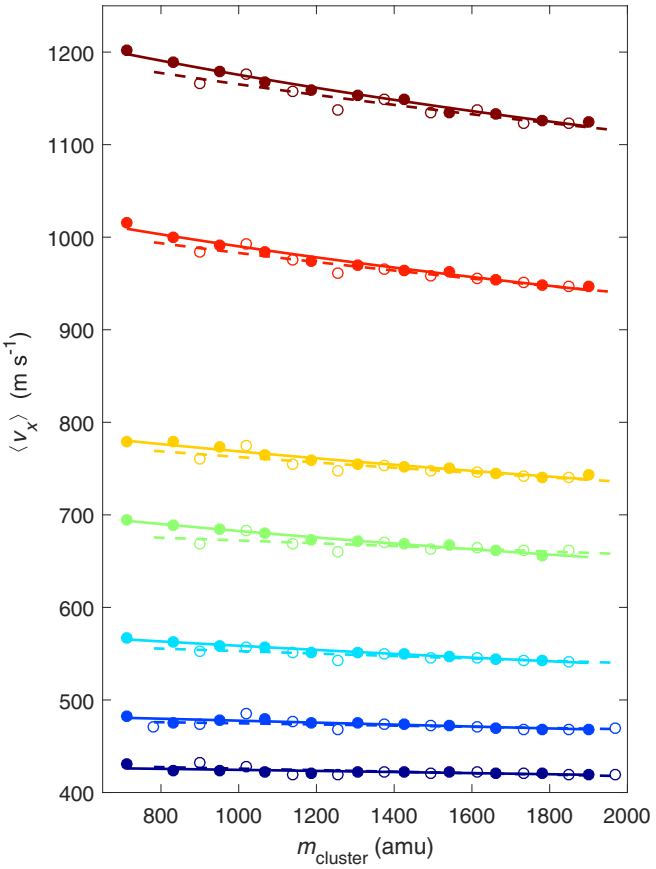

FIG. 4. Average cluster velocities $\langle v_x \rangle$ of Sn_N (closed circles) and $GaSn_N$ (open circles) in the molecular beam for nozzle temperatures 16 K (blue) to 300 K (maroon) (for color code see Fig. 2). Solid and dashed lines represent a flow model adopted from Ref. [43] [Eq. (12) therein] for Sn_N and $GaSn_N$, respectively.

describes the dependence of the cluster velocity on its mass m_{cluster} under the assumption of elastic collisions between the clusters and helium gas atoms

$$\langle v_x \rangle = \langle v_{\text{He}} \rangle \left[1 - \exp\left(-2N_{\text{col}} \frac{m_{\text{He}}}{m_{\text{He}} + m_{\text{cluster}}} \right) \right] \quad (3)$$

by taking the net number of accelerating collisions during the expansion N_{col} into account [43]. For the Sn_N and $GaSn_N$ clusters studied here, values between $N_{\text{col}} \approx 800$ and 400 result for 16 and 300 K, respectively, which is on the same order of magnitude as values determined for Co_N clusters of similar mass [43] but not sufficient for a thermalization of the vibrational modes with the He gas in the expansion [13]. Note that N_{col} is the number of collisions *during the adiabatic expansion*, while in the Introduction the number of collisions inside the cryogenically cooled nozzle *before the expansion* was estimated at 10^4. The increasing values of N_{col} for decreasing nozzle temperatures indicate a smaller velocity slip in the expansion [43]. This was already observed by comparing the cluster velocity with the expected helium velocity shown in Fig. 3. A large velocity slip indicates incomplete relaxation of the internal degrees of freedom of the clusters during the expansion. The temperature of the internal degrees of freedom will be discussed in more detail in Secs. V and VI.

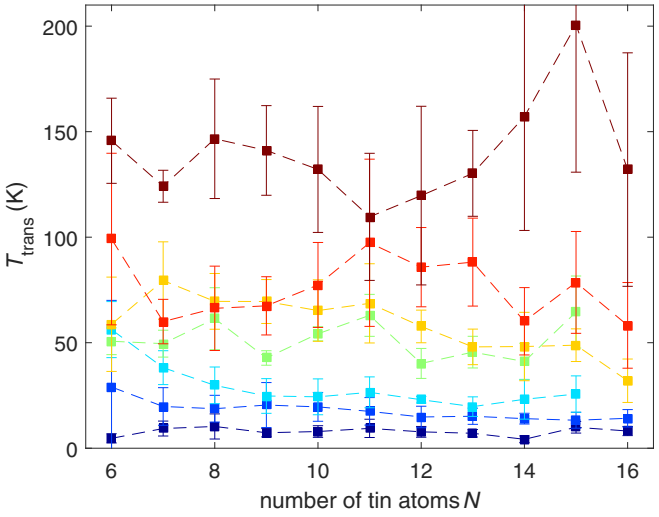

FIG. 5. Translational temperature for Sn_N clusters with $N =$ 6–16 and $T_{\text{nozzle}} =$ 16–300 K, extracted from Eq. (2). Error bars are standard deviations from at least three experimental runs. The dashed lines should be understood as a guide to the eye. The average velocities can also be extracted for the less stable doped $GaSn_N$ clusters, but the determination of T_{trans} is challenging due to worse beam stability. It is presumed that T_{trans} should be similar.

B. Translational temperature T_{trans}

The translational temperatures of the Sn_N clusters are extracted from the measured velocity distributions in Fig. 2 according to Eq. (2) and shown in Fig. 5 (note the considerations in Sec. II C). The uncertainty is relatively large due to moderate beam stability; however, it becomes clear that T_{trans} is significantly lower than T_{nozzle} for all temperatures in the range from 16 to 300 K. For example, for $T_{\text{nozzle}} = 16$ K, the mean value of T_{trans} for the Sn_N clusters with $N =$ 6–16 is 8 ± 2 K. However, we cannot distinguish the effect from the fixed photoionization time on T_{trans} (see Sec. II C) from translational cooling in the adiabatic expansion. Translational cooling was observed for small Co_N clusters in a quite similar laser vaporization source [43], which is why it seems conclusive that also the small Sn_N clusters studied here undergo translational cooling in the adiabatic expansion. No significant trend of T_{trans} with cluster mass can be deduced for the small-size range of the observed clusters.

V. ROTATIONAL TEMPERATURE

The rotational dynamics of an isolated cluster traveling through an inhomogeneous field affects its dipole moment orientation and thus the observable deflection caused by the Stark or Zeeman effect [35,36,56,57]. We choose the $GaSn_{11}$ cluster here because the simulated beam profiles for the GM structure from quantum chemical calculations fit the electric deflection data well, which indicates that the correct isomer was found. Additionally, practically no superatomic behavior was observed in the magnetic deflection experiments even for the lowest nozzle temperature, which makes it easier to observe a molecular-beam asymmetry, which will be utilized to estimate the rotational temperature.

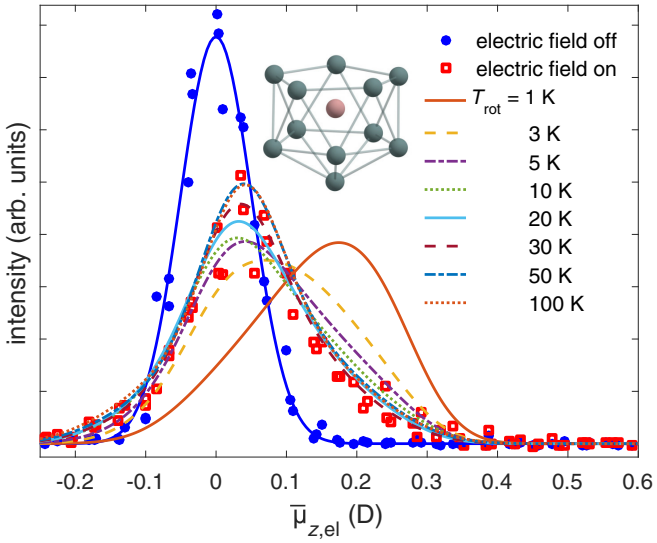

FIG. 6. Electric deflection profile for $GaSn_{11}$ at $T_{nozzle} = 16$ K and a deflection voltage of 24 kV. The GM structure with $S = \frac{1}{2}$ and the results from MD simulations for $T_{rot} = 1$–100 K are shown.

The electric dipole moment for a rigid cluster is fixed in the body-fixed coordinate frame and thus the rotational dynamics of a classical rotor with an electric dipole moment in an electric field can be calculated by solving the Euler equations in a molecular dynamics (MD) simulation [58]. Note that even for $T_{rot} = 1$ K, if a Boltzmann distribution with a rotational constant of $B_{rot} = 4.4 \times 10^{-26}$ J ($GaSn_{11}$) is considered, the states with rotational quantum number $R = 20$ have the largest population and states up to $R = 40$ are significantly populated. Thus, the classical approach in the MD simulation is still valid [35].

Figure 6 shows a molecular-beam profile of an electric deflection experiment on $GaSn_{11}$ and the results from MD simulations for different rotational temperatures T_{rot}. In the range of $T_{rot} = 10$–30 K, the difference in the shape of the molecular-beam profile is small and all curves fit the experimental data points rather well ($R^2 = 0.95$–0.96). The simulations for 50 and 100 K give comparable results and cannot be excluded ($R^2 = 0.94$). For $T_{rot} < 5$ K, the average deflection increases significantly and the beam profile tilts to positive values of $\overline{\mu}_{z,el}$. The strongly increased deflection for lower values of T_{rot} can be explained by comparing the energy for an orientation of the permanent electric dipole moment μ_{el} in the electric field $E = 10^7$ V m^{-1} with the thermal energy $k_B T_{rot}$. These two energies become equal for $T_{rot} = 0.6$ K if the electric dipole moment of $\mu_{el} = 0.26$ D for $GaSn_{11}$ from density-functional theory is taken into account. When $k_B T_{rot} < \mu_{el} E$, it would be expected that most clusters are aligned in the field and an average deflection with $\overline{\mu}_{z,el} = \mu_{el}$ would be observed [59]. The comparison of experiment and simulations indicates that $T_{rot} = 5$ K should be a lower bound to the rotational temperature. Considering uncertainties in the predicted electric dipole moments from quantum chemical calculations of up to 10–15 % [58], the lower bound of T_{rot} could also be 1–2 K smaller.

Also magnetic beam deflection is affected by the degree of rotational excitation. It was shown previously for gadolinium-doped tin clusters that an asymmetry in beam deflection profiles, or more precisely a tailing in the direction of the field gradient, is due to clusters in states with small values of R, i.e., rotationally cold clusters [60]. Figure 7 shows the experimental deflection data for $T_{nozzle} = 16$ and 30 K for $GaSn_{11}$. The tailing in the direction of the magnetic field gradient extends clearly beyond $\overline{\mu}_{z,mag} = 1\mu_B$, which would correspond to a Landé factor $g = 2$. The GM structure of $GaSn_{11}$ from quantum chemical calculations is nearly a symmetric rotor with C_{5v} symmetry and electronic spin $S = \frac{1}{2}$ (see the inset in Fig. 6). Thus, the g tensor can be anisotropic. The value of $\mu_{z,mag}$ then depends on the cluster orientation in the magnetic field, which explains why no discrete peak at a defined value of $\overline{\mu}_{z,mag}$ is observed but a tailing which extends to at least $2\mu_B$. The intensity in the right wing of the beam profiles (gradient direction) is 6.8% and 7.6% of the total beam intensity for $T_{nozzle} = 16$ and 30 K, respectively. The absolute intensity in the left wing is subtracted to eliminate possible residual

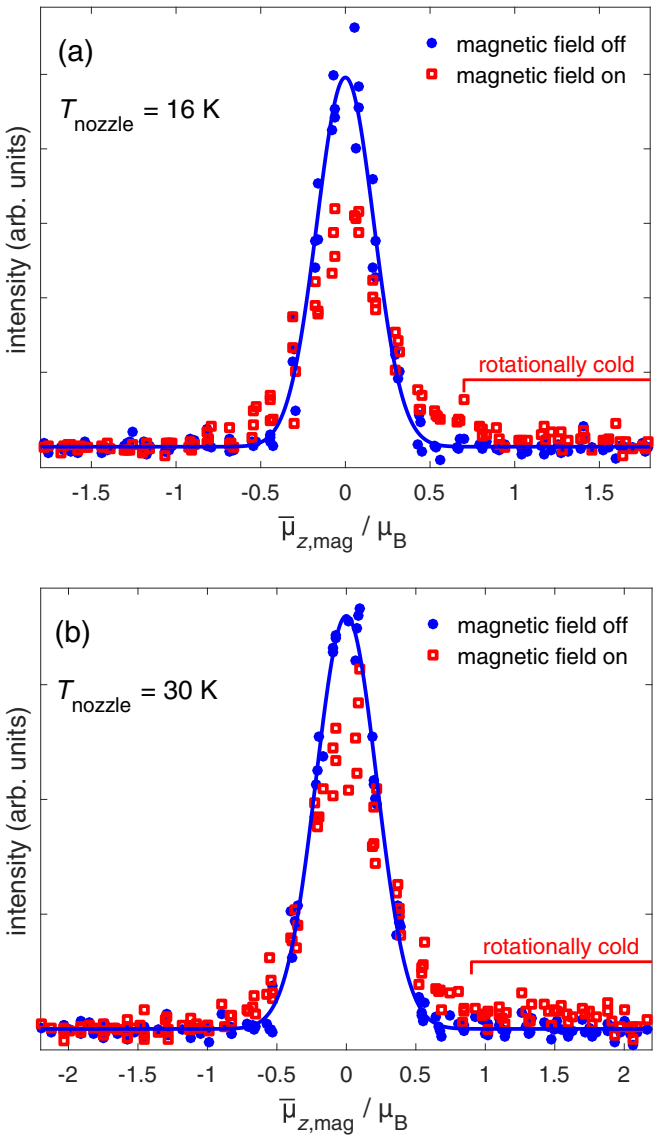

FIG. 7. Magnetic beam deflection profiles for $GaSn_{11}$ for (a) $T_{nozzle} = 16$ K and (b) $T_{nozzle} = 30$ K.

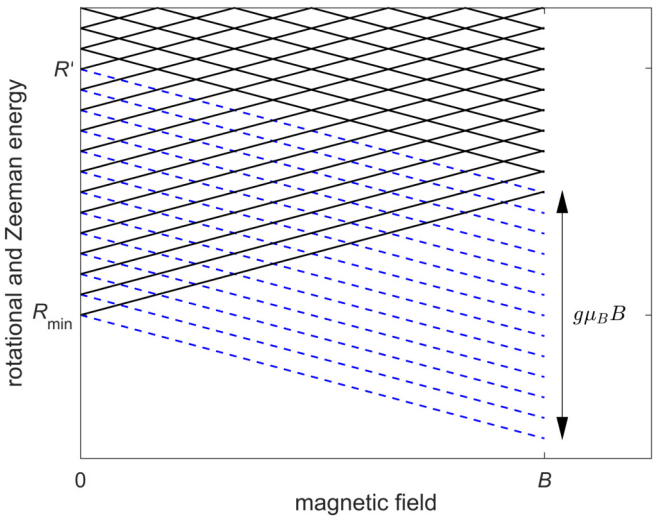

FIG. 8. Energy diagram for the spin and rotational states of an asymmetric rotor for $S = \frac{1}{2}$ and a given value of $J_{z,\mathrm{tot}}$. A simplified rotational energy level diagram is used where $E = nB_{\mathrm{rot}}R$, with $n \in \mathbb{N}_0$ reflecting the constant density of rotational states. Only every 50th state is shown for better visibility ($n = 0, 50, \ldots$). The blue dashed lines are the states which are designated as rotationally cold (see the text).

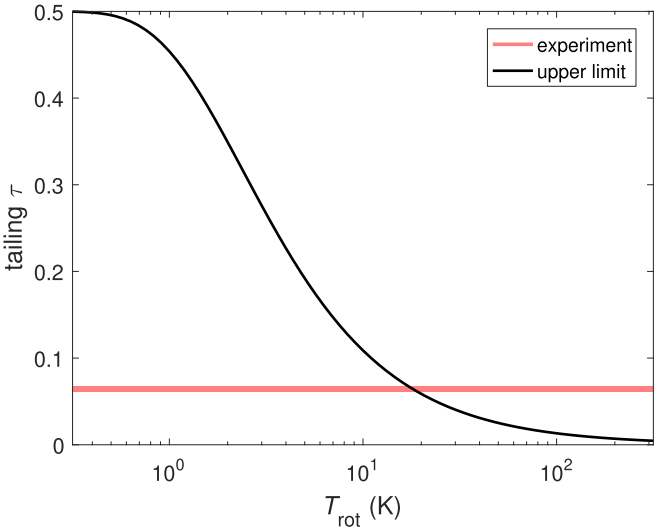

FIG. 9. Expected upper bound for the tailing from Eq. (5) (black line) compared to the experimentally found 6–6.8 % tailing (red).

superatomic clusters that would lead to intensity on both sides and thus 6% and 6.8% remain as the fractions of rotationally cold clusters. Vibrational excitation suppresses the tailing, which is why the molecular-beam asymmetry decreases below the detection limit for larger nozzle temperatures. Thus, the fraction of the rotationally cold clusters can be used to determine the rotational temperature.

We use a simple approach to estimate an upper bound for the rotational temperature for $T_{\mathrm{nozzle}} = 16$ and 30 K, considering only the rotational energy levels and Zeeman splitting in the vibrational ground state. For electronic spin $S = \frac{1}{2}$, there are two possible spin states $M_S = \pm\frac{1}{2}$ and thus only straight lines with slope $\pm 1/2g\mu_B$ originate from each rotational state in the Zeeman diagram. There is a lower bound of the rotational energy ($R = 0$) and thus, below the lowest possible energy state with positive slope, only states with negative slope exist (see Fig. 8). These states do not cross with any other states, which means that no spin flips are possible and thus the magnetic moments of clusters in these states are aligned to the field and produce large deflections with $\mu_{z,\mathrm{mag}} = 1/2g\mu_B$. As there is no upper bound to the rotational states, there are no states with positive slope that do not cross with other states and thus the described large deflections occur only in the direction of the magnetic field gradient.

Only crossings between states with the same total angular momentum $J_{z,\mathrm{tot}}$, containing contributions from rotation R_z and spin M_S, are avoided and facilitate spin flips. The smallest possible rotational quantum number R for a fixed value of $J_{z,\mathrm{tot}}$ is then $R_{\mathrm{min}} = |J_{z,\mathrm{tot}} - S|$. Rotational states with negative slope do not cross with other states at magnetic flux density B as long as the difference in rotational energy to the rotational state with R_{min} is smaller than the Zeeman splitting $g\mu_B B$. The highest rotational quantum number for which no level crossings occur at a given value of B is designated as R'. For a nearly spherical rotor, $E_{\mathrm{rot}}(R) \approx B_{\mathrm{rot}}R(R+1)$ and R' is determined from $E_{\mathrm{rot}}(R') - E_{\mathrm{rot}}(R_{\mathrm{min}}) = g\mu_B B$, which results in

$$R' = -\frac{1}{2} + \frac{1}{2}\sqrt{1 + 4\left[\frac{g\mu_B B}{B_{\mathrm{rot}}} + |J_{z,\mathrm{tot}} - S|(|J_{z,\mathrm{tot}} - S| + 1)\right]}. \tag{4}$$

The total amount of rotationally cold clusters is then calculated by counting the states that fulfill $R < R'$ for all possible values of $J_{z,\mathrm{tot}} = -R - S, \ldots, R + S$ with the Heaviside function $\theta(R - R')$. Dividing this by $2R + 1$ gives the corresponding fraction of clusters for a given value of R and $J_{z,\mathrm{tot}}$. Summing over all possible values for $J_{z,\mathrm{tot}}$ and R and weighting with the normalized distribution of rotational states $P(R)$ gives the total fraction of clusters with $R < R'$. For $S = \frac{1}{2}$, half of these clusters have a negative slope in the energy diagram and thus the expected fraction of clusters that are aligned to the field is

$$\tau = \frac{1}{2}\sum_{R=0}^{\infty} P(R) \sum_{J_{z,\mathrm{tot}}=-R-S}^{R+S} \frac{\Theta(R' - R)}{2R + 1}. \tag{5}$$

Figure 9 shows that with a Boltzmann distribution for $P(R)$, a value of $T_{\mathrm{rot}} \approx 20$ K must be assumed so that Eq. (5) gives an amount of about 6–6.8 % of tailing, which was observed in the magnetic deflection experiment. This value should be understood as an upper bound because vibrational excitation quenches the tailing and thus lower values of T_{rot} would be needed to reproduce the experimental results when some clusters in the experiment are vibrationally excited.

However, care must be taken when the rotational energy distribution is described by a single value for the temperature T_{rot}. It is known that the rotational energy distribution after an adiabatic expansion can possibly be nonthermal, i.e., does not follow a simple Boltzmann distribution, which is assumed in both the electric and magnetic simulations [61]. The reason

for this is that intramolecular energy redistribution is quite ineffective with rotational degrees of freedom. In contrast, the vibration-vibration energy exchange is quite effective, which ensures a thermal distribution for vibrational degrees of freedom after the adiabatic expansion [16]. Thus, the concept of describing the energy distribution with a single temperature is justified for T_{vib} but not necessarily for T_{rot}. However, spectroscopic results on small molecules in supersonic beams mostly showed that a Boltzmann distribution is a valid approximation [62]. Sometimes it has been observed that higher rotational states are overpopulated [61,63]. With the method described above, too large values of T_{rot} would be estimated, however, these values would still be a valid upper bound.

Extracting a definite value for the rotational temperature from the observed beam profiles is difficult for various reasons. (i) Quantum chemical calculations suggest that $GaSn_{11}$ has one low-lying vibrational mode at about 7 cm^{-1}, which would be excited for most clusters. However, especially such soft vibrational modes from quantum chemical calculations tend to be inaccurate. Furthermore, it is not quite clear how a single vibrational mode would affect the tailing. (ii) Gathering information on cluster properties from an asymmetry in molecular-beam profiles requires a very good linearity of the detector response over the observed deflection range. However, the magnetic field gradient is calibrated with a deflection experiment on the spin-$\frac{3}{2}$ bismuth atom, which shows that intensity variations are smaller than 10% over a range of at least ± 3 mm, which is even larger than the deflection range for $GaSn_N$ clusters (± 2 mm). Therefore, the observation of about ten times more tailing in the right compared to the left wing of the beam profile is definitely significant.

To conclude here, we can give a lower bound for the rotational temperature of $GaSn_{11}$ for $T_{\mathrm{nozzle}} = 16$ K from electric deflection experiments and an upper bound from the magnetic deflection, i.e., $5 \leqslant T_{\mathrm{rot}} \leqslant 20$ K. For $T_{\mathrm{nozzle}} = 30$ K, a similar fraction of the clusters is found to be rotationally cold in the magnetic deflection experiment, which implies a comparable value of T_{rot}. However, the comparison of MD simulation with electric deflection data works best for the lowest temperatures because (i) cluster are slower and the measured deflection is larger and (ii) a rigid rotor is assumed in the MD simulation. Therefore, we cannot give a reliable lower bound for $T_{\mathrm{nozzle}} = 30$ K. A similar range of values for T_{rot} was found in earlier works on tetrel clusters from our group where T_{rot} was also estimated from the comparison of electric deflection experiments with MD simulations [35–37,64] or from the contribution of the permanent dipole moment to the electric polarizability within an adiabatic polarization mechanism [34,65,66].

VI. VIBRATIONAL TEMPERATURE

The determination of vibrational temperatures from magnetic deflection experiments on small metal clusters was demonstrated for $MnSn_{12}$ [5]. It was found that the vibrational temperature is equal to the nozzle temperature for $T_{\mathrm{nozzle}} \geqslant 30$ K. The situation is quite different for the $GaSn_{12}$ cluster with $S = \frac{1}{2}$ compared to $MnSn_{12}$ even though both are endohedral cage clusters. For icosahedral $MnSn_{12}$ clusters with electronic spin $S = \frac{5}{2}$ and pure spin magnetism, i.e., $g = 2$, in their vibrational ground state, spin-rotation coupling is very small. Thus, no spin flips occur at most level crossings, which leads to superatomic magnetic response in Stern-Gerlach and effective refocusing in double-deflection experiments. Jahn-Teller active vibrational modes reduce the molecular symmetry and induce spin-rotation coupling which leads to spin flips on avoided level crossings (see [5] for more details) and thus both superatomic magnetic deflection and refocusing efficiency are quenched [67]. Such vibrationally excited clusters show Brillouin-like behavior, i.e., a small deflection in the direction of the magnetic field gradient. On the contrary, $GaSn_{12}$ possesses a rather large orbital angular momentum. The contribution of spin-orbit coupling to spin-rotation coupling is expected to be much larger than the total value of spin-rotation coupling for $MnSn_{12}$ [57,67] and thus spin flips occur at most level crossings in the deflection and refocusing experiment, even in the vibrational ground state [68]. Still, superatomic magnetic response is observed in the vibrational ground state because the rotational energy level density for a spherical rotor with electronic spin $S = \frac{1}{2}$ is nine times smaller compared to $S = \frac{5}{2}$. Vibrational excitation leads to an increase of the density of states [60]. For an ensemble of harmonic oscillators, the rate at which the density of vibrational states increases is ϵ^{γ}, with energy ϵ and the number of excited vibrational modes γ [57]. Therefore, the number of level crossings a cluster experiences in the field increases with vibrational excitation, which leads to an enhanced number of spin flips and thus Brillouin-like behavior. Consequently, not only the Jahn-Teller active but all vibrational modes must be considered for $GaSn_{12}$.

While for $MnSn_{12}$ with $S = \frac{5}{2}$, each Jahn-Teller active mode induces spin flips [5], $GaSn_{12}$ can show superatomic response in the magnetic deflection experiment even when one or a few vibrational modes are excited. Vibrational excitation can be taken explicitly into account in a microscopic model considering vibrational, rotational, and Zeeman energy. From each possible combination of vibrational quantum numbers of the $3N - 6$ normal modes of the cluster, rotational and spin states emerge. For the spherical rotor $GaSn_{12}$ it is assumed that spin flips occur on all avoided level crossings, i.e., crossings between energy levels of different rotational and spin quantum numbers where angular momentum conservation holds. For a randomly generated ensemble of at least 10 000 clusters with Boltzmann-distributed rotational and vibrational energy, the average of the magnetic dipole moment $\overline{\mu}_{z,\mathrm{mag}}$ is calculated for all states with the same total angular momentum $J_{z,\mathrm{tot}}$. The number of level crossings N_{cross} depends on the total density of states and the change of the magnetic flux density while the cluster travel through the magnetic field. For $N_{\mathrm{cross}} \gg 1$, many spin flips occur and thus the spread of $\overline{\mu}_{z,\mathrm{mag}}$ and also the molecular-beam broadening will be small. When N_{cross} is zero, superatomic response is observed, i.e., a splitting of the molecular beam in $2S + 1$ beamlets. For small but nonzero values of N_{cross}, the value of $\overline{\mu}_{z,\mathrm{mag}}$ is calculated as the weighted mean value of $N_{\mathrm{cross}} + 1$ values of the possible values of $\mu_{z,\mathrm{mag}} = d\epsilon/dB$ weighted with the corresponding density of states. For more details on the model, refer to Ref. [60]. In double-deflection experiments in analogy to Ref. [69], it was found that 15% of the clusters in the molecular beam are highly polar and

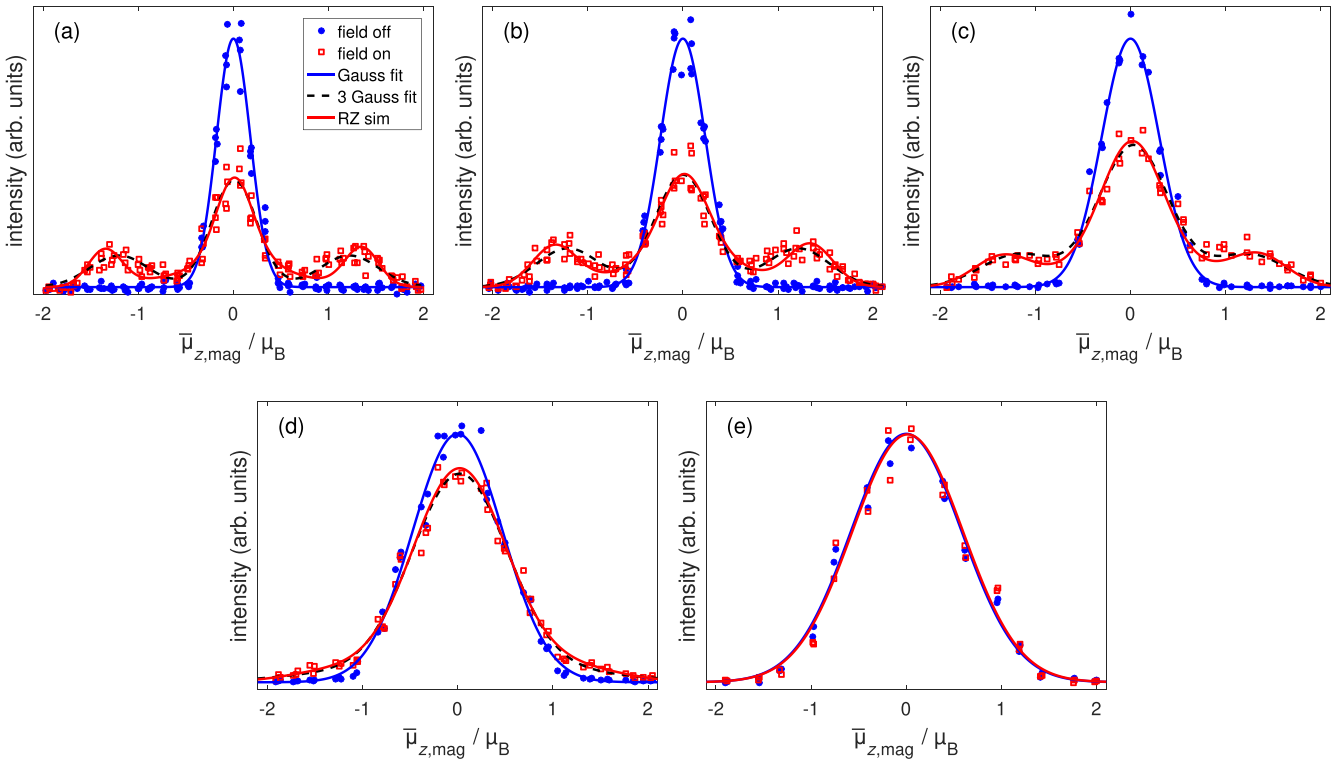

FIG. 10. Deflection data from Stern-Gerlach experiments on $GaSn_{12}$ for (a) $T_{nozzle} = 16\,K$, (b) $T_{nozzle} = 30\,K$, (c) $T_{nozzle} = 50\,K$, (d) $T_{nozzle} = 70\,K$, and (e) $T_{nozzle} = 100\,K$. Blue circles and red squares show the cluster intensity with magnetic field switched off and on, respectively. The blue solid and black dashed lines show fits with one and three equidistant Gaussians, respectively. Rotation-Zeeman (RZ) simulation results for $T_{vib} = 47$, 47, 52, 64, and 100 K are shown as red lines (for details see the text). Note that the profiles with field off become broader for increasing temperature despite the beam dimensions being equal for all experiments because $\overline{\mu}_{z,mag} \propto v_x^2$ [compare Eq. (1)].

thus do not show superatomic response even in the vibrational ground state. Therefore, for the simulations in Fig. 10, 15% of the molecular-beam profile is assumed to show Brillouin-like magnetic response, irrespective of the vibrational temperature (see Appendix B). Therefore, only for the remaining 85%, the beam profile is treated within the described microscopic model.

A value of $T_{rot} = 10\,K$ is chosen here; however, rotational temperatures in the estimated range of 5–20 K do not affect the beam profiles of $GaSn_{12}$ significantly as the rotationally cold clusters in the vibrational ground state show superatomic magnetic response anyway. With rotational constant B_{rot} and the 33 vibrational frequencies from quantum chemical calculations, the vibrational temperature T_{vib} remains the only unknown parameter. Choosing T_{vib} such that the simulated beam profile matches the experimentally observed beam profile leads to the values shown in Table I next to the superatomic fraction determined from a fit of three equidistant Gaussians (dashed black lines in Fig. 10). While T_{vib} is close to T_{nozzle} for the higher nozzle temperatures, there is no significant decrease of T_{vib} below 50 K. This is essentially similar to the observations for $MnSn_{12}$; however, deviations of T_{vib} from T_{nozzle} occur for somewhat higher temperatures. In the experiment with $T_{nozzle} = 100\,K$, no superatomic behavior is observed. In the simulations, the superatomic fraction is below the detection limit of a few percent for $T_{vib} \geqslant 80\,K$, which means that this is a lower bound for the vibrational temperature.

It should be stressed here that the determination of T_{vib} depends on the vibrational frequencies from our quantum chemical calculations. For the GM of $GaSn_{12}$ [see Fig. 1(a)], the lowest vibrational modes are found at $\tilde{\nu} = 47\,cm^{-1}$ (triply degenerate). We estimate the error in T_{vib} from the uncertainty of $\tilde{\nu}$ to be about 5 K.

As mentioned above, the number of level crossings depends on the change of the magnetic flux density ΔB on the molecular-beam path through the field. The clusters are deflected in the gradient field, which leads to ΔB of a few tens of milliteslas. However, when the magnetic field and the molecular-beam path are not aligned perfectly orthogonal, ΔB would significantly increase, which leads to more spin flips and fewer superatomic clusters in the Stern-Gerlach

TABLE I. Superatomic fraction from a fit of three equidistant Gaussian functions and vibrational temperature T_{vib} determined by taking the rotation-Zeeman model into account.

T_{nozzle} (K)	Superatomic fraction (%)	T_{vib} (K)
16	51	47
30	51	47
50	39	52
70	13	64
100		$\geqslant 80$

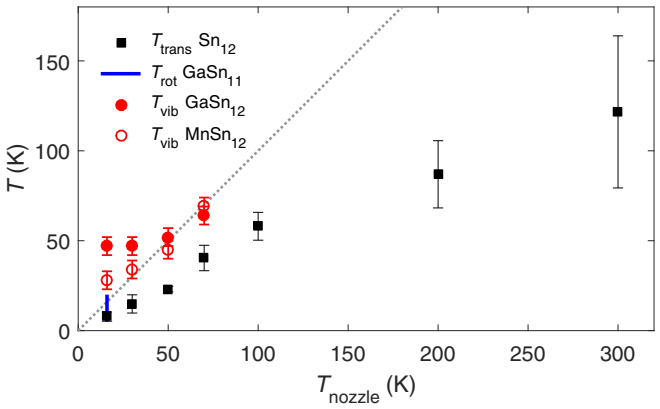

FIG. 11. Translational, rotational, and vibrational temperatures depending on nozzle temperature for Sn_{12} and $GaSn_N$ with $N = 11, 12$ in comparison to earlier data on $MnSn_{12}$ [5,70], using the same cluster source. Note that, due to the measuring procedure, the values of T_{trans} should be understood as a lower bound.

experiment. Thus, smaller values of T_{vib} would be needed to match the simulation to the experimentally observed beam profiles. In the simulations shown in Fig. 10, only ΔB through deflection is considered.

VII. DISCUSSION AND CONCLUSION

The determined values for translational, rotational, and vibrational temperatures are summarized in Fig. 11. The values obtained for T_{trans} are significantly colder than the nozzle temperature for 16–300 K, which means that the velocity distributions are quite narrow. The estimated upper and lower bounds of T_{rot} are just above T_{trans} for $T_{nozzle} = 16$. In contrast, T_{vib} is near the nozzle temperature for $T_{nozzle} > 50$ K ($GaSn_{12}$) or $T_{nozzle} > 30$ K ($MnSn_{12}$), but significantly larger than T_{trans} and T_{rot} for lower temperatures. This demonstrates that while translational and probably also rotational degrees of freedom are significantly cooled in the adiabatic expansion, the vibrations are much less influenced. The deviation of T_{vib} from T_{nozzle} for very low temperatures indicates that the vibrations are not fully thermalized with the cryogenically cooled beam nozzle, even though the number of collisions with the helium gas should suffice for thermalization. Possible approaches to improve on this issue are using a longer nozzle or increasing the helium pressure. However, both parameters cannot be varied easily because they strongly affect the molecular-beam intensity and stability.

Our observations are in line with earlier molecular-beam studies utilizing different techniques for the determination of temperatures, for example, rotationally resolved spectroscopy on metal dimers [19] and small lithium clusters [31] or delayed ionization experiments on small niobium clusters [27] or magnetic deflection experiments [71]. On the other side, there is no evidence that internal energy (especially vibrational energy) is transferred into translational energy in the expansion, which was observed in an in-depth study of the velocity distribution of cobalt clusters Co_N ($N = 6 - 60$) by van der Tol and Janssens [43]. However, as we cannot distinguish translational cooling in the adiabatic expansion and the effect from the fixed photoionization delay which leads to lower values of T_{trans}, a combined approach determining (i) the velocity distribution of all clusters in the molecular beam [43] and (ii) rotational and translational temperatures for some cluster species in a molecular beam from the same laser vaporization source could resolve the issue on how internal energy is redistributed in the adiabatic expansion.

ACKNOWLEDGMENTS

The authors acknowledge financial support from the Deutsche Forschungsgemeinschaft through Grant No. SCHA 885/16-1. Calculations for this research were conducted on the Lichtenberg high performance computer of TU Darmstadt.

APPENDIX A: DETERMINATION OF THE LANDÉ FACTOR FOR $GaSn_{12}$

The beamlets assigned to the superatomic fractions in Fig. 10(a) are significantly broader than the molecular-beam profile with magnetic field switched off and also broader than the one observed for $AlSn_{12}$ [68,69]. This makes it difficult to determine a value for the Landé factor g because for exclusively superatomic magnetic response, the width of the beamlets should not differ from the beam profile without field. However, it is obvious that the outer edges of these beamlets around $\overline{\mu}_{z,mag} = \pm 1.6\mu_B$ are rather sharp compared to the inner edges towards the central peak, which is why the sum of three Gaussians in Fig. 10(a) (black dashed line) does not quite fit the shape of the experimental data. Instead, the simulated beam profile with $g = 2.7$ reproduces the sharp outer edges of the superatomic beamlets nicely. The more shallow intensity decrease towards the central peak is due spin flips on avoided level crossings. If the electronic spin flips halfway through the magnet, zero deflection is expected. In contrast, when the spin state changes right in the beginning or the end of the magnetic field, a deflection somewhat below the expected value for $M_S = \pm\frac{1}{2}$ will be observed, which would lead to a broadening of the superatomic beamlets towards the central peak. The intensity of the experimental beam profile in this region [$|\overline{\mu}_{z,mag}| = 0.6\mu_B$–$0.9\mu_B$ in Fig. 10(a)] is underestimated by the simulation, which could be due to fluctuations of the magnetic flux density in the deflection field because of imperfections in the magnet pole shoes or slight misalignment. Thus, a value of $g = 2.7$ seems reasonable for $GaSn_{12}$.

APPENDIX B: POLAR FRACTION OF $GaSn_{12}$ CLUSTERS

Electric and electric-magnetic double-deflection experiments for $GaSn_{12}$ are shown in Fig. 12. The beam profile without field is described by a Gaussian function in good approximation. By applying an electric field, the beam profile shifts in direction of the field gradient and a small tailing is observed. Here two Gaussian functions are necessary to describe the beam profile properly. This suggests that two fractions are present in the molecular beam which can be assigned to a polar and a nonpolar isomer [69]. To investigate these two fractions more closely, a combination of the electric and magnetic beam-deflection experiment is carried out. Here the two fractions get spatially separated in the electric field so that only the nonpolar fraction passes the following magnetic

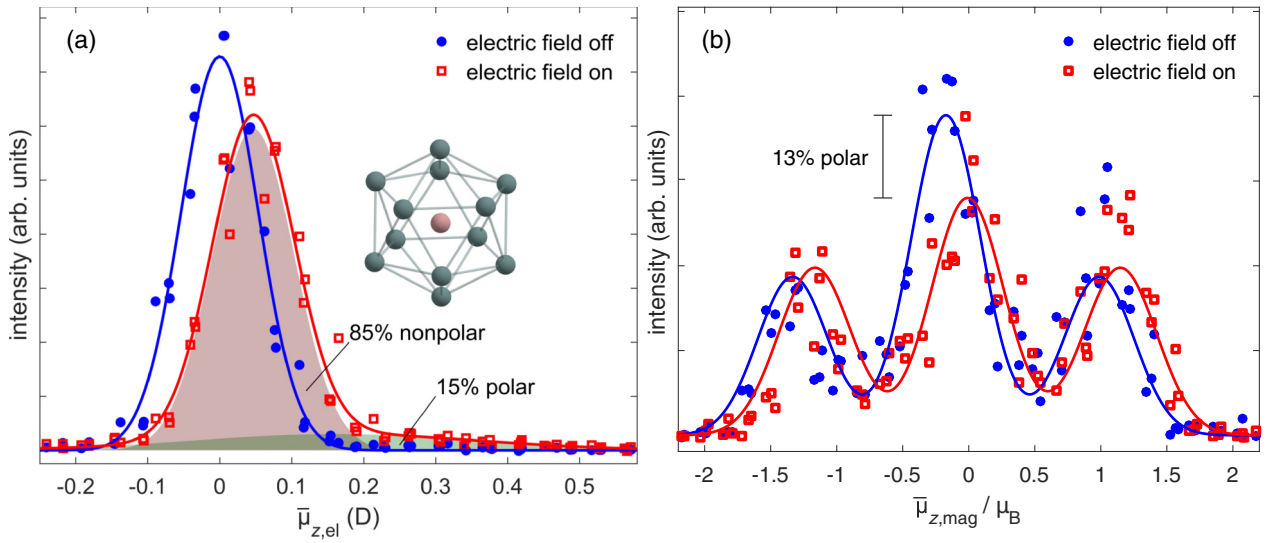

FIG. 12. (a) Electric and (b) electric-magnetic double-deflection experiment on $GaSn_{12}$ for $T_{nozzle} = 16$ K. The (nonpolar) GM structure in (a) is a slightly distorted icosahedron with T_h symmetry. In (b) the magnetic field is switched on permanently. For more experimental details, see Ref. [69].

field. By filtering out the polar fraction, only the beamlet in the center of the beam profile decreases, which demonstrates that the polar clusters do not show superatomic magnetic response. Some polar clusters are still present after selection, which is why the intensity reduction in the double-deflection experiment corresponds to a slightly smaller number of polar clusters than the electric deflection experiment. Therefore, a value of 15% of the $GaSn_{12}$ clusters in the molecular beam is assigned to a highly polar, nonsuperatomic isomer, which is taken into account for the rotation-Zeeman calculations in Sec. VI. For more details on the double-deflection experiment, see Ref. [69].

[1] T. G. Dietz, M. A. Duncan, D. E. Powers, and R. E. Smalley, J. Chem. Phys. **74**, 6511 (1981).
[2] M. A. Duncan, Rev. Sci. Instrum. **83**, 041101 (2012).
[3] G. N. Makarov, Phys. Usp. **51**, 319 (2008).
[4] I. M. L. Billas, A. Châtelain, and W. A. de Heer, Science **265**, 1682 (1994).
[5] U. Rohrmann and R. Schäfer, Phys. Rev. Lett. **111**, 133401 (2013).
[6] C. van Dijk, J. Bowlan, W. A. de Heer, T. Rasing, and A. Kirilyuk, J. Phys. Chem. C **119**, 11153 (2015).
[7] R. Kusche, T. Hippler, M. Schmidt, B. von Issendorff, and H. Haberland, Eur. Phys. J. D **9**, 1 (1999).
[8] M. Schmidt, C. Ellert, W. Kronmüller, and H. Haberland, Phys. Rev. B **59**, 10970 (1999).
[9] T. Bachels, H.-J. Güntherodt, and R. Schäfer, Phys. Rev. Lett. **85**, 1250 (2000).
[10] J. Woenckhaus and J. A. Becker, Rev. Sci. Instrum. **65**, 2019 (1994).
[11] J. P. Bucher, D. C. Douglass, and L. A. Bloomfield, Rev. Sci. Instrum. **63**, 5667 (1992).
[12] I. M. L. Billas, J. A. Becker, and W. A. de Heer, Z. Phys. D **26**, 325 (1993).
[13] J. Westergren, H. Grönbeck, A. Rosén, and S. Nordholm, J. Chem. Phys. **109**, 9848 (1998).
[14] E. Oger, R. Kelting, P. Weis, A. Lechtken, D. Schooss, N. R. M. Crawford, R. Ahlrichs, and M. M. Kappes, J. Chem. Phys. **130**, 124305 (2009).
[15] G. Scoles, *Atomic and Molecular Beam Methods*, 1st ed. (Oxford University Press, Oxford, 1988).
[16] G. Sanna and G. Tomassetti, *Introduction to Molecular Beams Gas Dynamics* (Imperial College Press, London, 2005).
[17] X. Xu, S. Yin, R. Moro, A. Liang, J. Bowlan, and W. A. de Heer, Phys. Rev. Lett. **107**, 057203 (2011).
[18] A. Diaz-Bachs, M. I. Katsnelson, and A. Kirilyuk, New J. Phys. **20**, 043042 (2018).
[19] J. B. Hopkins, P. R. R. Langridge-Smith, M. D. Morse, and R. E. Smalley, J. Chem. Phys. **78**, 1627 (1983).
[20] J. R. Woodward, S. H. Cobb, and J. L. Gole, J. Phys. Chem. **92**, 1404 (1988).
[21] P. Y. Cheng and M. A. Duncan, Chem. Phys. Lett. **152**, 341 (1988).
[22] G. A. Bishea and M. D. Morse, J. Chem. Phys. **95**, 8779 (1991).
[23] G. A. Bishea, C. A. Arrington, J. M. Behm, and M. D. Morse, J. Chem. Phys. **95**, 8765 (1991).
[24] C. A. Arrington and M. D. Morse, J. Phys. Chem. **112**, 16182 (2008).
[25] M. F. Jarrold and K. M. Creegan, Chem. Phys. Lett. **166**, 116 (1990).
[26] M. Förstel, W. Schewe, and O. Dopfer, Angew. Chem. Int. Ed. **58**, 3356 (2019).
[27] B. A. Collings, A. H. Amrein, D. M. Rayner, and P. A. Hackett, J. Chem. Phys. **99**, 4174 (1993).
[28] A. O'Keefe, J. J. Scherer, A. L. Cooksy, R. Sheeks, J. Heath, and R. J. Saykally, Chem. Phys. Lett. **172**, 214 (1990).

[29] G. A. Bishea, N. Marak, and M. D. Morse, J. Chem. Phys. **95**, 5618 (1991).

[30] G. A. Bishea, J. C. Pinegar, and M. D. Morse, J. Chem. Phys. **95**, 5630 (1991).

[31] J. Blanc, M. Broyer, J. Chevaleyre, P. Dugourd, H. Kühling, P. Labastie, M. Ulbricht, J. P. Wolf, and L. Wöste, Z. Phys. D **19**, 7 (1991).

[32] M. Keil, H.-G. Krämer, A. Kudell, M. Baig, J. Zhu, W. Demtröder, and W. Meyer, J. Chem. Phys. **113**, 7414 (2000).

[33] D. T. Vituccio, O. Golonzka, and W. E. Ernst, J. Mol. Spectrosc. **184**, 237 (1997).

[34] S. Schäfer, B. Assadollahzadeh, M. Mehring, P. Schwerdtfeger, and R. Schäfer, J. Phys. Chem. A **112**, 12312 (2008).

[35] S. Heiles, S. Schäfer, and R. Schäfer, J. Chem. Phys. **135**, 034303 (2011).

[36] U. Rohrmann, P. Schwerdtfeger, and R. Schäfer, Phys. Chem. Chem. Phys. **16**, 23952 (2014).

[37] D. A. Götz, A. Shayeghi, R. L. Johnston, P. Schwerdtfeger, and R. Schäfer, Nanoscale **8**, 11153 (2016).

[38] S. Schäfer, M. Mehring, R. Schäfer, and P. Schwerdtfeger, Phys. Rev. A **76**, 052515 (2007).

[39] U. Rohrmann, S. Schäfer, and R. Schäfer, J. Phys. Chem. A **113**, 12115 (2009).

[40] L. P. Maguire, S. Szilagyi, and R. E. Scholten, Rev. Sci. Instrum. **75**, 3077 (2004).

[41] R. E. Scholten, Rev. Sci. Instrum. **78**, 026101 (2007).

[42] H. Haberland, U. Buck, and M. Tolle, Rev. Sci. Instrum. **56**, 1712 (1985).

[43] J. van der Tol and E. Janssens, Phys. Rev. A **102**, 022806 (2020).

[44] M. Jäger, R. Schäfer, and R. L. Johnston, Nanoscale **11**, 9042 (2019).

[45] P. Giannozzi, S. Baroni, N. Bonini, M. Calandra, R. Car, C. Cavazzoni, D. Ceresoli, G. L. Chiarotti, M. Cococcioni, I. Dabo *et al.*, J. Phys.: Condens. Matter **21**, 395502 (2009).

[46] A. M. Rappe, K. M. Rabe, E. Kaxiras, and J. D. Joannopoulos, Phys. Rev. B **41**, 1227 (1990).

[47] J. P. Perdew, K. Burke, and M. Ernzerhof, Phys. Rev. Lett. **77**, 3865 (1996).

[48] M. Methfessel and A. T. Paxton, Phys. Rev. B **40**, 3616 (1989).

[49] J. P. Perdew, J. Tao, V. N. Staroverov, and G. E. Scuseria, J. Chem. Phys. **120**, 6898 (2004).

[50] B. Metz, H. Stoll, and M. Dolg, J. Chem. Phys. **113**, 2563 (2000).

[51] M. Gleditzsch, T. M. Fuchs, and R. Schäfer, J. Phys. Chem. A **123**, 1434 (2019).

[52] M. Gleditzsch, L. F. Pasteka, D. A. Götz, A. Shayeghi, R. L. Johnston, and R. Schäfer, Nanoscale **11**, 12878 (2019).

[53] M. Valiev, E. J. Bylaska, N. Govind, K. Kowalski, T. P. Straatsma, H. J. J. van Dam, D. Wang, J. Nieplocha, E. Apra, T. L. Windus, and W. A. de Jong, Comput. Phys. Commun. **181**, 1477 (2010).

[54] F. Neese, WIREs Comput. Mol. Sci. **2**, 73 (2012).

[55] P. Milani and W. A. DeHeer, Rev. Sci. Instrum. **61**, 1835 (1990).

[56] P. Dugourd, R. Antoine, M. Abd El Rahim, D. Rayane, M. Broyer, and F. Calvo, Chem. Phys. Lett. **423**, 13 (2006).

[57] X. Xu, S. Yin, R. Moro, and W. A. de Heer, Phys. Rev. B **78**, 054430 (2008).

[58] S. Heiles and R. Schäfer, *Dielectric Properties of Isolated Clusters* (Springer, Dordrecht, 2014).

[59] D. J. Merthe and V. V. Kresin, J. Phys. Chem. Lett. **7**, 4879 (2016).

[60] T. M. Fuchs and R. Schäfer, Phys. Rev. A **100**, 012512 (2019).

[61] N. Dam, C. Liedenbaum, S. Stolte, and J. Reuss, Chem. Phys. Lett. **136**, 73 (1987).

[62] W. L. Meerts, G. ter Horst, J. M. L. J. Reinartz, and A. Dymanus, Chem. Phys. **35**, 253 (1978).

[63] T. E. Gough and R. E. Miller, J. Chem. Phys. **78**, 4486 (1983).

[64] D. A. Götz, S. Heiles, R. L. Johnston, and R. Schäfer, J. Chem. Phys. **136**, 186101 (2012).

[65] S. Schäfer and R. Schäfer, Phys. Rev. B **77**, 205211 (2008).

[66] S. Schäfer, S. Heiles, J. A. Becker, and R. Schäfer, J. Chem. Phys. **129**, 044304 (2008).

[67] T. M. Fuchs and R. Schäfer, Phys. Rev. A **98**, 063411 (2018).

[68] T. M. Fuchs and R. Schäfer, Phys. Chem. Chem. Phys. **23**, 11334 (2021).

[69] F. Rivic, T. M. Fuchs, and R. Schäfer, Phys. Chem. Chem. Phys. **23**, 9971 (2021).

[70] U. Rohrmann, Das magnetische Verhalten Mangan-dotierter Zinncluster, Ph.D. thesis, Technische Universität Darmstadt, 2014.

[71] I. M. L. Billas, A. Châtelain, and W. A. de Heer, J. Magn. Magn. Mater. **168**, 64 (1997).